LA-UR-81-2795

CONF-820601--1

MASTER

TITLE: RESPONSE OF CONTAINMENT VESSELS TO EXPLOSIVE BLAST LOADING

AUTHOR(S): T. A. Duffey, M-4 Visiting Staff Member
R. R. Karpp, M-4
T. R. Neal, M-4

SUBMITTED TO: Pressure Vessel and Piping Division (ASME) Conference
Orlando, Florida
June 27 to July 1, 1982

LA-UR--81-2795

DE82 000570



University of California

LOS ALAMOS SCIENTIFIC LABORATORY
Post Office Box 1663 Los Alamos, New Mexico 87545
An Affirmative Action/Equal Opportunity Employer

Form No. 836 R3
St. No. 2629
12/78

UNITED STATES
DEPARTMENT OF ENERGY
CONTRACT W-7405-ENG. 36

# RESPONSE OF CONTAINMENT VESSELS TO EXPLOSIVE BLAST LOADING

T. A. Duffey,* Member ASME
Visiting Staff Member
Los Alamos National Laboratory
Group M-4, MS940
Los Alamos, New Mexico 87545

R. R. Karpp
Staff Member
Los Alamos National Laboratory
Group M-4, MS940
Los Alamos, New Mexico 87545

T. R. Neal
Group Leader
Los Alamos National Laboratory
Group M-4, MS940
Los Alamos, New Mexico 87545

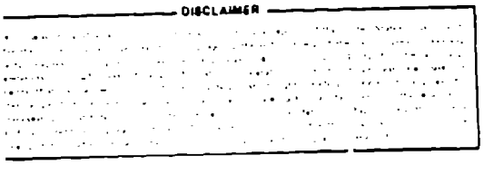


## ABSTRACT

The response of steel containment vessels to the blast loading produced by the detonation of high explosives is investigated by experiments, computations, and analysis. The vessels are thin-wall shell structures that are nearly spherical. All explosive charges are solid spheres, centrally initiated and centrally positioned within the vessels. Most of the work concerns vessels that contain, in addition to the explosive charge, air at ambient or reduced pressures.

One-dimensional, Lagrangian, finite-difference calculations are used to study the blast phenomenon and the details of the loading pulse applied to the vessel wall. The results are verified by comparisons with pressure gauge records. In addition,

*Permanent Address: Department of Mechanical Engineering, University of New Mexico, Albuquerque, New Mexico 87131.

vessel response to the pressure loading is calculated by both finite-difference and finite-element computer codes. The two-dimensional motion, which occurs after significant wave interactions have taken place in the test vessels, can be simulated, with reasonable accuracy, by finite-element calculations. This result indicates that a predictive technique and, therefore, a design tool appear to be available with these standard calculational methods.

## INTRODUCTION

A number of investigations have been reported in the literature on the response of spherical shells or containment vessels subjected to internal blast loading.[1-7] Interest in such spherical containment vessels stems primarily from testing or disposal of explosive-related devices as well as containment of accidental explosions. As discussed in Reference 7, high-repetition applications, such as repeated testing of explosive components, generally suggest design on the basis of elastic-only behavior of the vessel or shell,[1,2,5,7] whereas low repetition vessel applications, such as containment of accidental explosions, suggest elastic-plastic designs for efficient material utilization.[3,4,6]

The present study represents a more detailed investigation of the elastic containment problem, including both a refined accounting of the pressure loading on the vessel wall as well as the corresponding structural response of the vessel.

First, the one-dimensional symmetric motion of a thin spherical shell is analyzed, and the maximum strain occurring in the shell wall as a function of the loading-pulse duration is determined. For a given impulse, the maximum strain decreases rapidly when the loading duration exceeds about one-fourth of a natural one-dimensional vibration period. This fact emphasizes one obvious mechanism of blast-wave mitigation: if a filler material temporally spreads the blast wave, a decrease in the maximum strain will result.

Next, the details of the blast loading applied to the vessel

wall are analyzed with the aid of one-dimensional finite-difference code calculations. Each pressure pulse has a fairly complicated structure caused by shock-wave reflections between the vessel wall and the air-explosive interface. Comparisons between pressure-gauge records and the calculations show good qualitative agreement. By using the calculated pressure pulse in conjunction with the equation describing the one-dimensional motion of a thin spherical shell, the strain history occurring in a vessel can be calculated. The computed strain histories agree well with strain-gage measurements during the first half-cycle of motion. The calculated peak strain is about 20 percent high. The response of the test vessels after about a half-cycle of spherical motion is predominantly two-dimensional (axially symmetric). To analyze the two-dimensional response, the ADINA finite-element code is used. Comparisons between strain-gage records and finite-element calculations show good agreement. The small-scale test vessels used in this program are nearly axially symmetric with relatively large flanges around their equators. For these calculations, the strains occurring at the strain-gage locations are quite sensitive to the boundary conditions prescribed at the flanges. The flanges cause large axially symmetric perturbations in the initially spherical vessel motion. Calculations and test results show that this perturbation can cause a drastic strain amplification, which is due mostly to bending waves. Thus, a well-designed vessel should avoid this type of perturbation.

## ONE-DIMENSIONAL MOTION OF A THIN SPHERICAL SHELL

Consider the spherical shell segment shown in Figure 1. The shell thickness is denoted by h, its average radius by R, and its density by $\rho$. The driving pressure on the interior wall is a function of time denoted by P(t). For spherically symmetric motion, the balanced biaxial stress is denoted by $\sigma$ and the radial displacement by u. Within the thin-shell approximation, the equation of motion in the radial direction is [1]

$$\rho \frac{d^2u}{dt^2} + \frac{2\sigma}{R} = \frac{P(t)}{h} \quad . \tag{1}$$

Hooke's law for biaxial stress is

$$\sigma = \frac{E}{1-\nu} \varepsilon \quad . \tag{2}$$

where E and $\nu$ denote Young's modulus and Poisson's ratio, respectively, and $\varepsilon$ denotes the biaxial strain ($\varepsilon = u/R$). A combination of Equations (1) and (2) produces the equation governing the one-dimensional, linearly elastic motion of a thin spherical shell. The equation is

$$\frac{d^2u}{dt^2} + \omega^2 u = \frac{P(t)}{\rho h} \quad , \tag{3}$$

where

$$\omega^2 = \frac{2E}{\rho R^2 (1-\nu)} \quad .$$

The general solution of Equation (3) is

$$u = u_0 \cos \omega t + \frac{\dot{u}_0}{\omega} \sin \omega t + \frac{1}{\rho h \omega} \int_0^t P(\tau) \sin \omega(t-\tau) d\tau \quad , \tag{4}$$

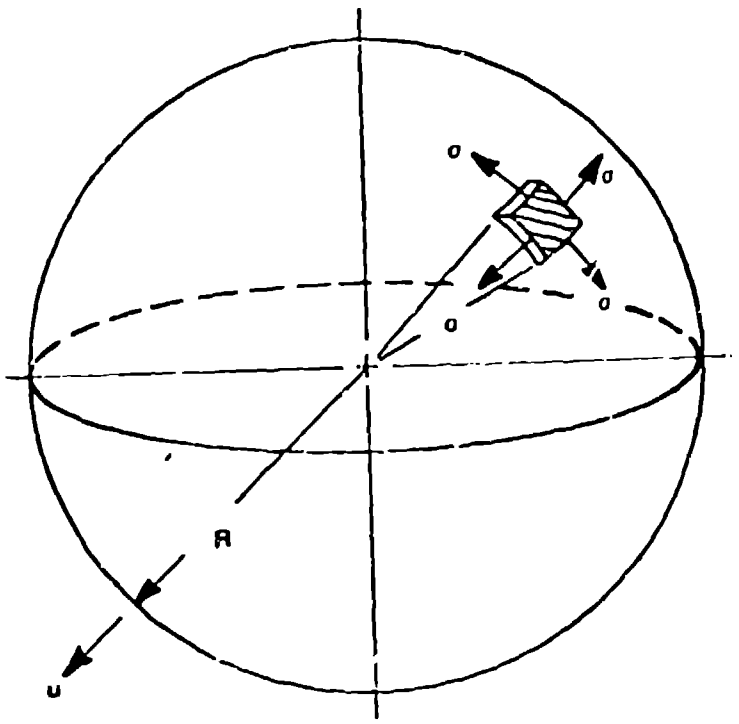


Fig. 1. Segment of a spherical shell.

where $u_0$ is the initial radial displacement and $\dot{u}_0$ is the initial radial velocity.

Consider a spherical shell acted upon by the rectangular pressure pulse illustrated in Figure 2. The magnitude of the internal pressure pulse is $P_0$ and its duration is $\Delta T$. The solutions for zero initial conditions ($u_0 = \dot{u}_0 = 0$), obtained from Equation (4), are

$$u = \frac{P_0}{\rho h \omega^2} [1 - \cos \omega t] \text{ for } 0 \leq t \leq \Delta T \quad , \tag{5}$$

and

$$u = \frac{P_0}{\rho h \omega^2} [\cos \omega(t - \Delta T) - \cos \omega t] \text{ for } t > \Delta T \quad . \tag{6}$$

The solution for a purely impulsive load, that is a load applied over a very short time period, may be obtained from Equation (6) by assuming that $\Delta T$, the duration of loading, is much smaller than $T = 2\pi/\omega$, the vessel's natural vibration period. For an impulsive load, Equation (6) reduces to

$$u = \frac{I}{\rho h \omega} \sin \omega t \quad , \tag{7}$$

where

$$I = \int_0^{\Delta T} P(t)\, dt = P_0\, \Delta T$$

is the specific impulse of the loading. From Equation (7), the maximum strain induced by an impulsive load may be written as

$$\varepsilon_{max} = \frac{I}{h\sqrt{\rho}\,\sqrt{\frac{2E}{1-\nu}}} \quad . \tag{8}$$

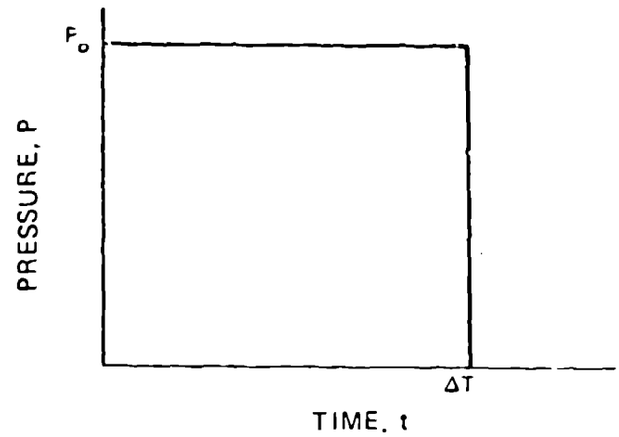


(a) RECTANGULAR PRESSURE PULSE

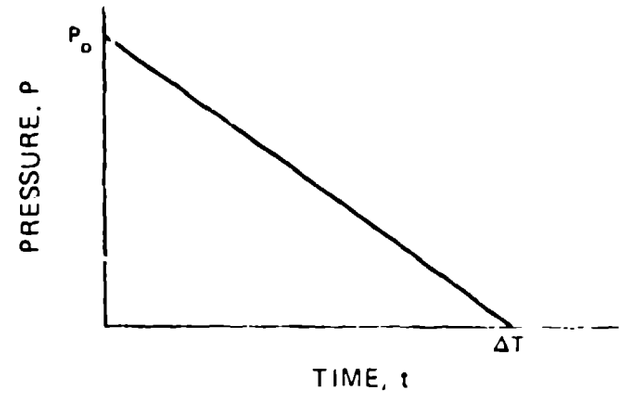


(b) TRIANGULAR PRESSURE PULSE

Fig. 2. Pressure pulses considered in the analysis of shell motion.

Equation (8) is true for any shaped pressure pulse as long as the loading duration is small, that is, the maximum strain is only a function of the applied impulse. However, when a pressure pulse is applied over a time period that is not small compared to T, the maximum strain induced in the shell depends upon both the pressure pulse shape and the total impulse. This feature is illustrated by again considering the motion of a spherical shell excited by the application of a rectangular pressure pulse. From Equations (5) and (6), the strain history may be written as

$$\varepsilon(t) = \frac{I}{h\sqrt{\rho}\sqrt{\frac{2E}{1-\nu}}} f(\omega t, \omega\Delta T) \quad , \tag{9}$$

where

$$f(\omega t, \omega\Delta T) = \frac{1}{\omega\Delta T}[1 - \cos \omega t] \text{ for } 0 \leq t \leq \Delta T$$

and

$$f(\omega\Delta T) = \frac{1}{\omega\Delta T}[\cos \omega(t - \Delta T) - \cos \omega t] \text{ for } t > T \quad .$$

If $f_{max}(\omega\Delta T)$ represents the maximum value of $f(\omega t, \omega\Delta T)$ as time varies, the maximum strain can be expressed, from Equation (9), as

$$\varepsilon_{max} = \frac{I}{h\sqrt{\rho}\sqrt{\frac{2E}{1-\nu}}} f_{max}(\omega\Delta T) \quad . \tag{10}$$

Equation (10) gives the maximum strain occurring in the shell as a function of the specific impulse, I, and the loading duration, $\Delta T$. The form of the function $f_{max}(\omega\Delta T)$ can be determined from Equation (9) for a rectangular pressure pulse. This function, plotted in Figure 3, indicates the sensitivity of the peak strain

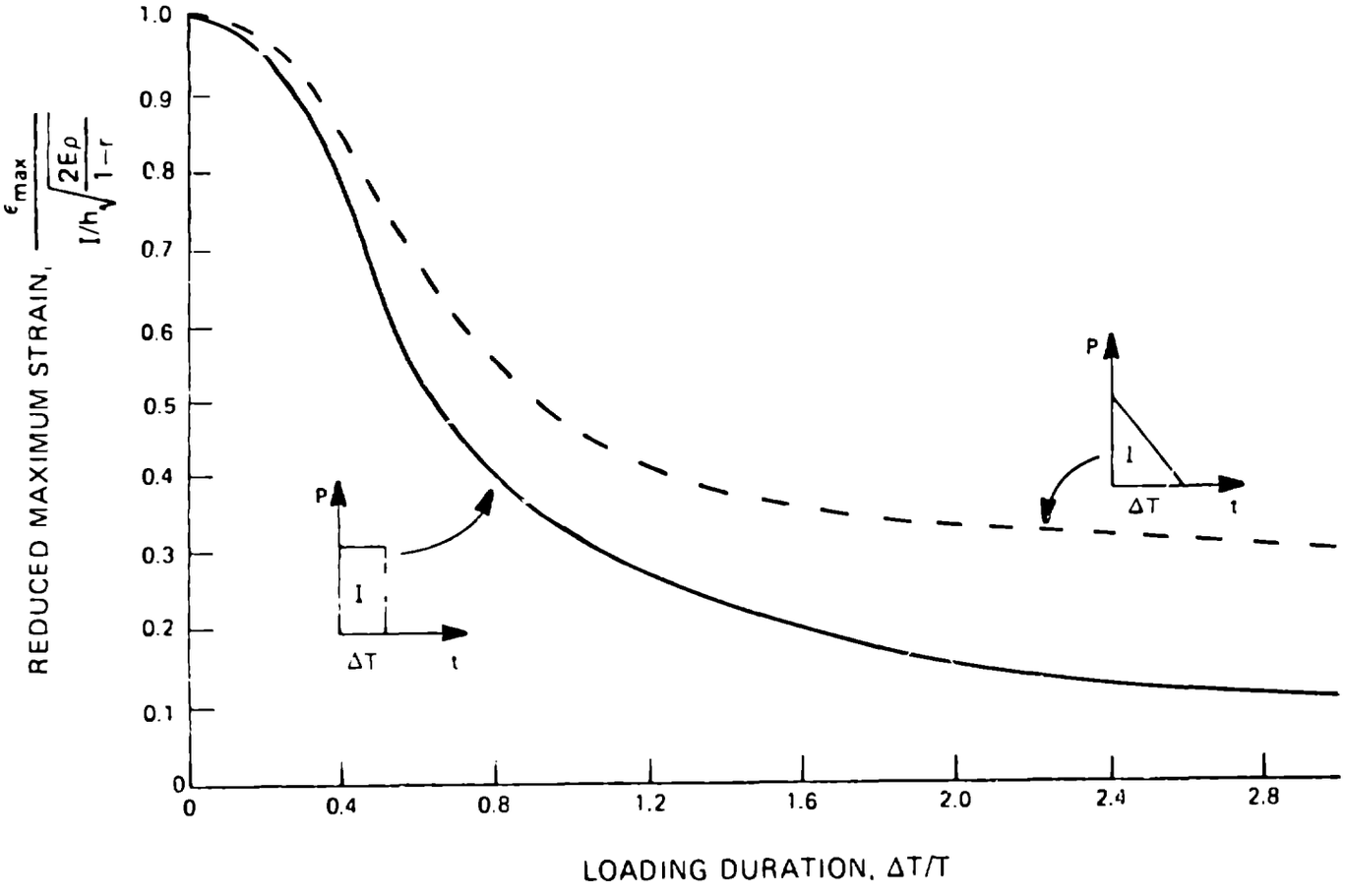


Fig. 3. Effect of pressure pulse shape on the maximum strain of a spherical shell.

in a spherical shell to the loading duration of a rectangular pulse. The maximum strain occurring in the shell decreases rapidly for loading durations greater than T/4.

The above derivation, carried out for the triangular pressure pulse shown in Figure 2, also leads to Equation (10) with, of course, a different expression for $f_{max}(\omega\Delta T)$. This expression is also plotted in Figure 3. Comparing the two curves in Figure 3 gives an idea of the sensitivity of shell response to pulse shape.

Summarising the results, the maximum circumferential strain is proportional to the applied impulse and inversely proportional to the wall thickness, the square root of the density, and the square root of twice the biaxial stress modulus, $E/(1-\nu)$, as indicated by Equation (10). The maximum circumferential strain is also proportional to $f_{max}(\omega\Delta T)$, which accounts for the finite duration of the loading pulse. The function $f_{max}(\omega\Delta T)$ is different for pressure pulses of different shapes, and it is equal to unity for impulsive loadings. For loadings of longer duration, $f_{max}(\omega\Delta T)$ may be considerably less than unity. Thus, loadings of equal impulse may produce completely different peak strains. For a particular type of explosive charge, the loading duration depends upon both the relative size of the charge and the properties of the filler material that transmits the pressure pulse.

## PRESSURE LOADING ON VESSEL WALLS

### Calculation of Pressure Loading

To qualitatively understand the pressure loading on the vessel wall and to establish a predictive capability, computer hydrodynamic calculations of the motion of the explosive and filler material within the containment vessel were performed. In the calculations, spherical symmetry was assumed. The computer code used to perform them is based on a fairly common one-dimensional, Lagrangian, finite-difference technique similar to the one described by Fickett.[8] Initially, the explosive is assumed to be burned completely, and the distribution of properties within the explosive products is determined from the Taylor similarity solution.[9] In these calculations, the equation of state used to describe the explosive products is the JWL equation.[10] The filler material considered here is either air or a perfect vacuum. For air, a $\gamma$-law equation of state was used with $\gamma = 1.4$. The shell velocity is obtained by numerically integrating Equation (3) along with the numerical solution of the hydrodynamic equations. The results of a calculation involving a 25.4-mm-diam explosive charge of PBX-9404 in an air-filled, 352-mm-diam vessel are illustrated in Figure 4a. This figure is a plot of the position of several particles within the flow field as a function of time; it gives an idea of the wave motion set up within the vessel. Figure 4b, obtained from Figure 4a, indicates some of this wave motion. Shock wave positions are indicated by dotted lines. The main shock, M, is followed by a secondary shock,

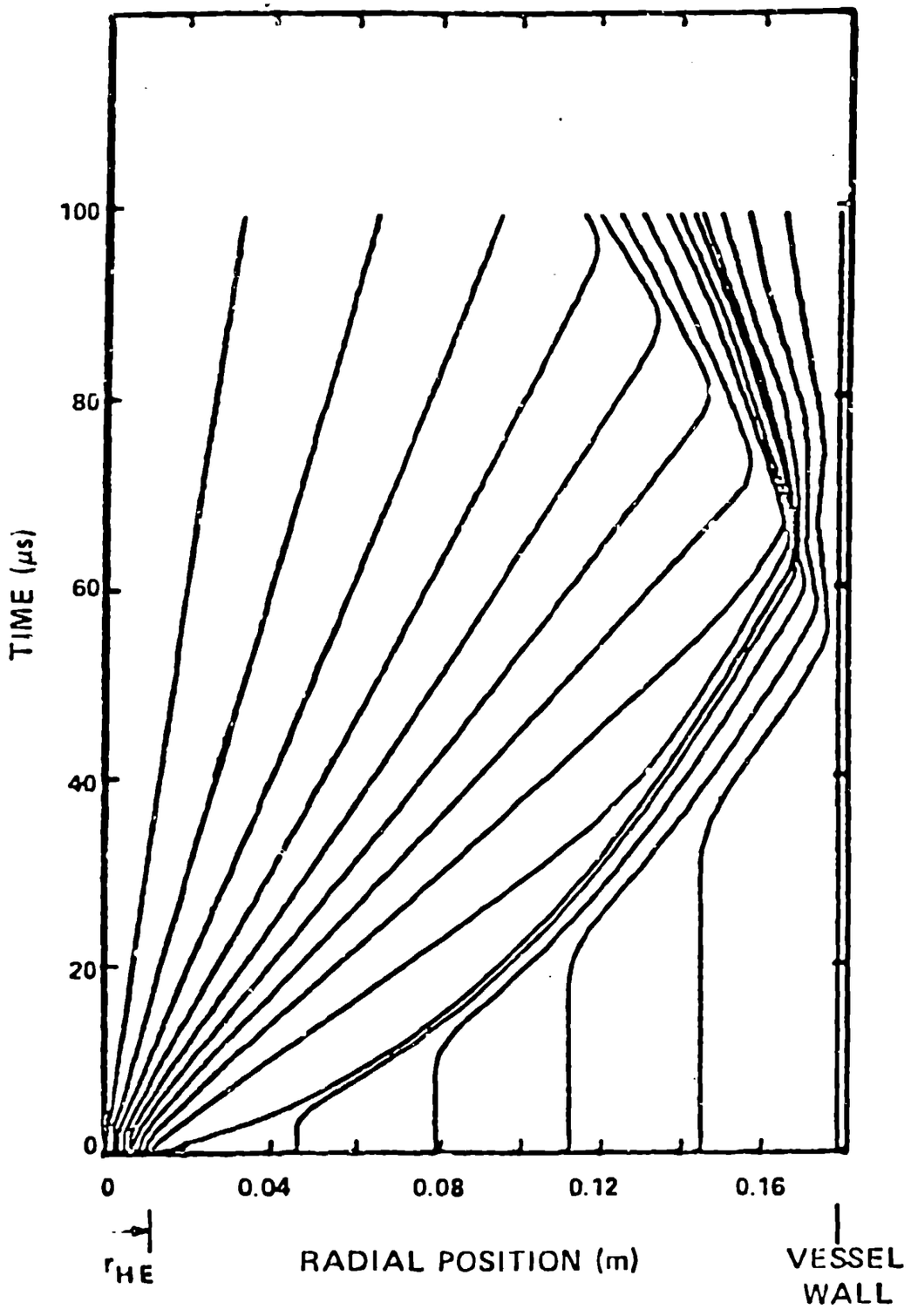


Fig. 4a. Plot of numerically calculated particle paths [25.4-mm-diam spherical explosive charge (HE) of mostly PBX-9404 in a 0.352-m-diam vessel filled with air at 79 kPa (0.78 atm) pressure].

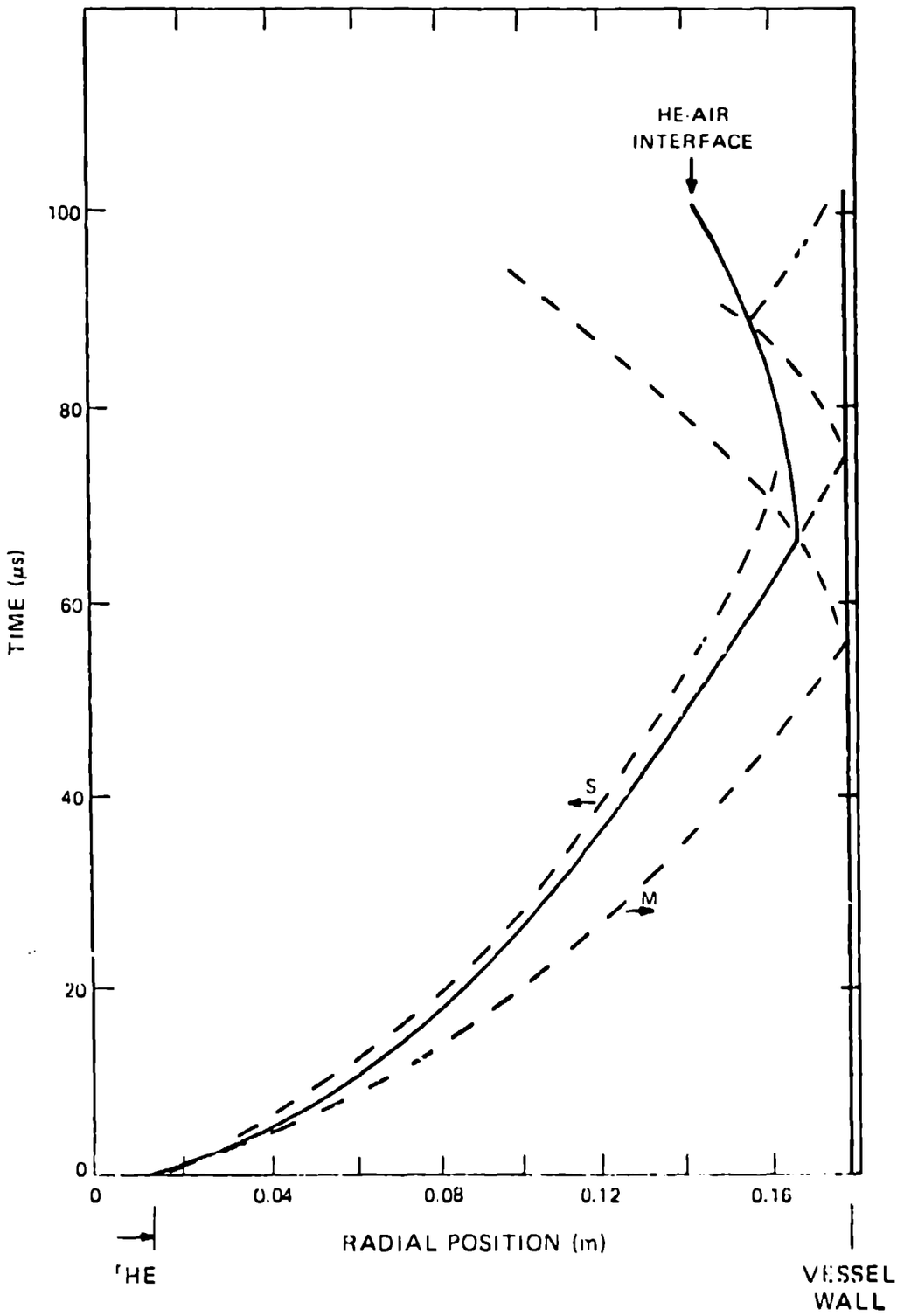


Fig. 4b. Location of some of the shock waves occurring in the flow of Figure 4a.

S, which propagates inward relative to the moving explosive products. The secondary shock, formed because of the spherically diverging flow discussed by Brode,[11] produces a high-density region between the secondary shock and the air-explosive interface. This condition is illustrated in Figure 5, where the pressure and density distributions are shown at 40 μs, shortly before the main shock reaches the vessel wall.

The main shock front reflects from the vessel wall at 53 μs and collides with the air-explosive interface at 63 μs, as indicated in Figure 4b. At that point, part of the wave is transmitted into the explosive products, but, because of the high-density region, another, substantial part is reflected into the air. The reflected part impinges on the vessel wall at 70 μs. Therefore, we would expect to see a second loading pulse applied to the vessel wall at this time. Figure 6 shows the calculated pressure pulse applied to the vessel wall for the first 200 μs. Here the initial pressure loading at 53 μs and the second pressure loading at 70 μs are apparent. The shock wave that causes the second loading continues to rebound between the interface and the vessel wall, but additional pressure pulses caused by its subsequent reflections are of negligible amplitude for this example.

The pressure on the vessel wall continues to drop until the main shock front is reflected from the center of symmetry and propagates out to the vessel wall. The reflected wave arrives at the vessel wall at 240 μs and produces the second major loading pulse. Figure 7 shows the arrival of the second major loading

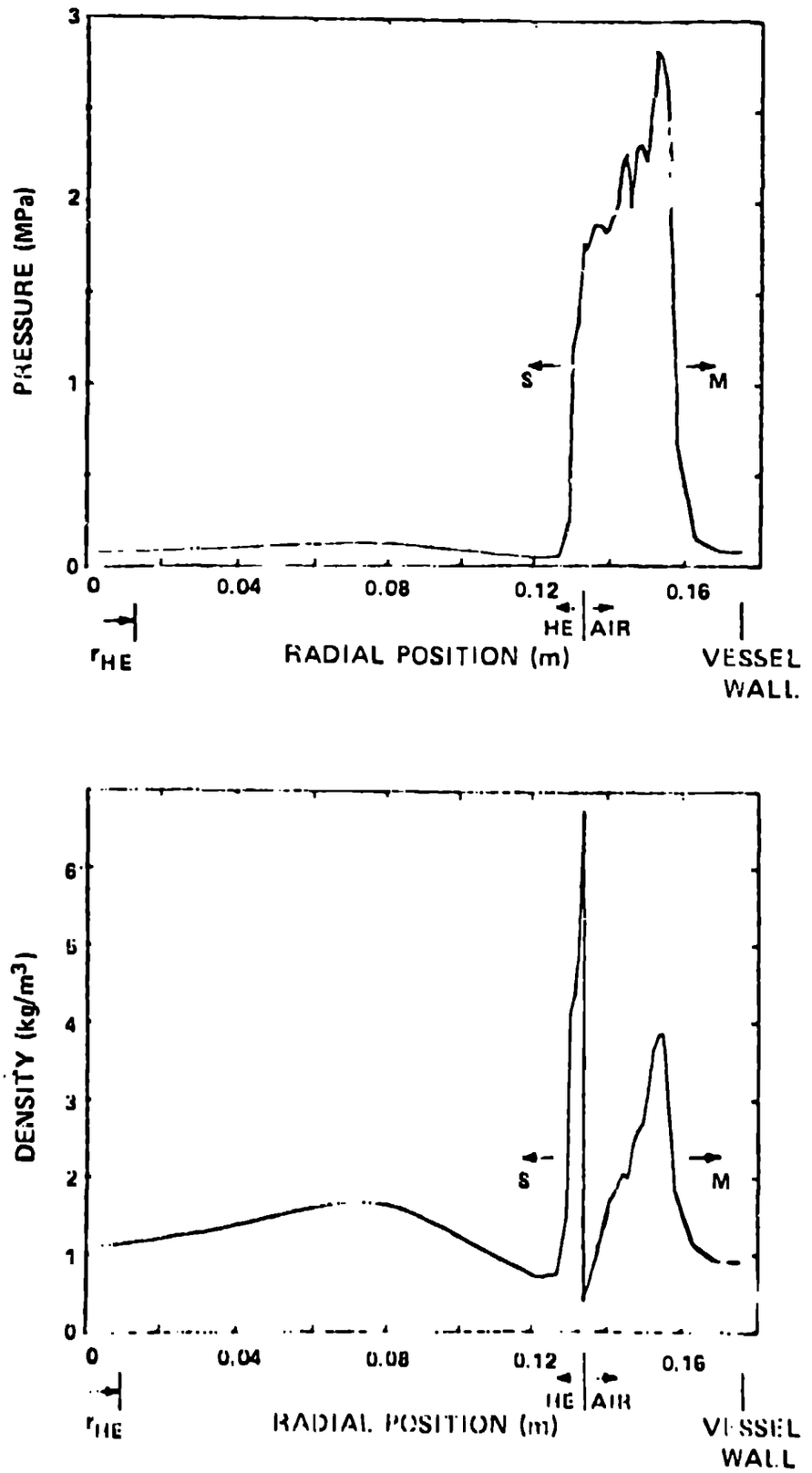


Fig. 5. Pressure and density distributions at 40 μs after explosive detonation (configuration indicated in Figure 4a).

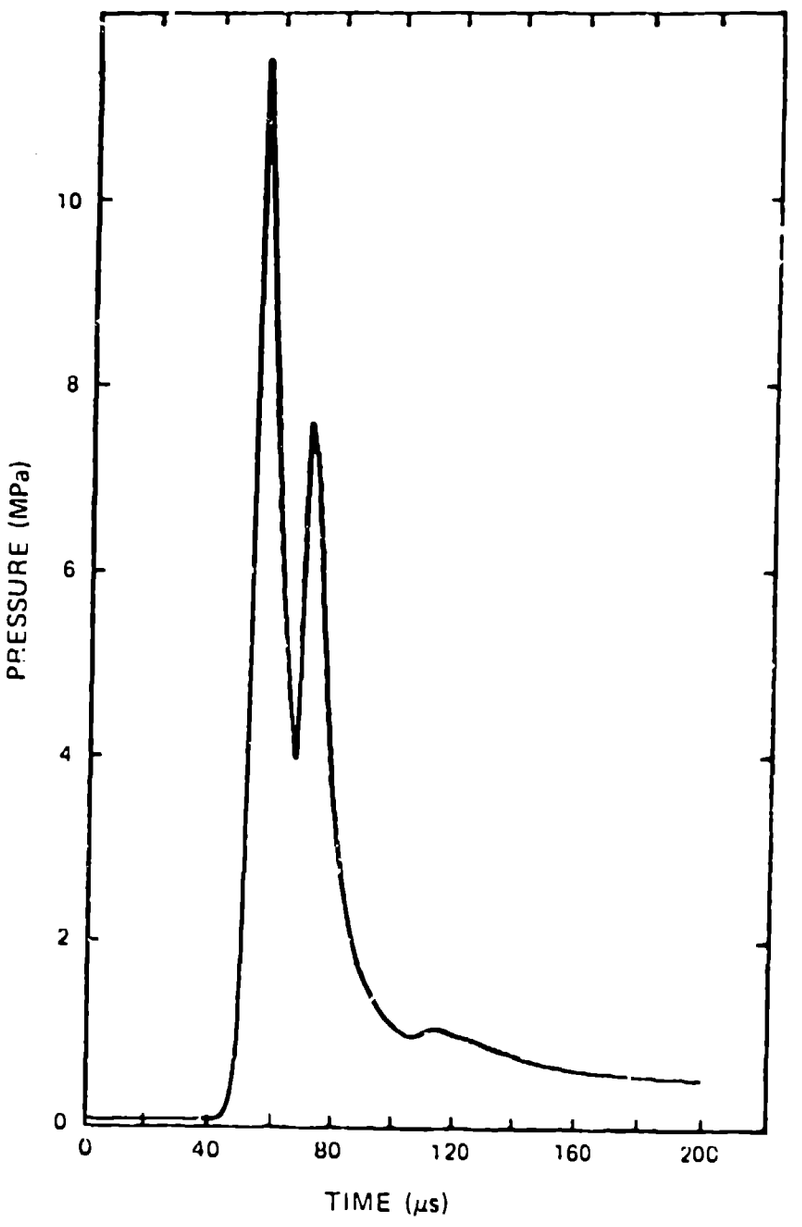


Fig. 6. Calculated pressure pulse acting on the vessel wall (0-200 μs, configuration indicated in Figure 4a).

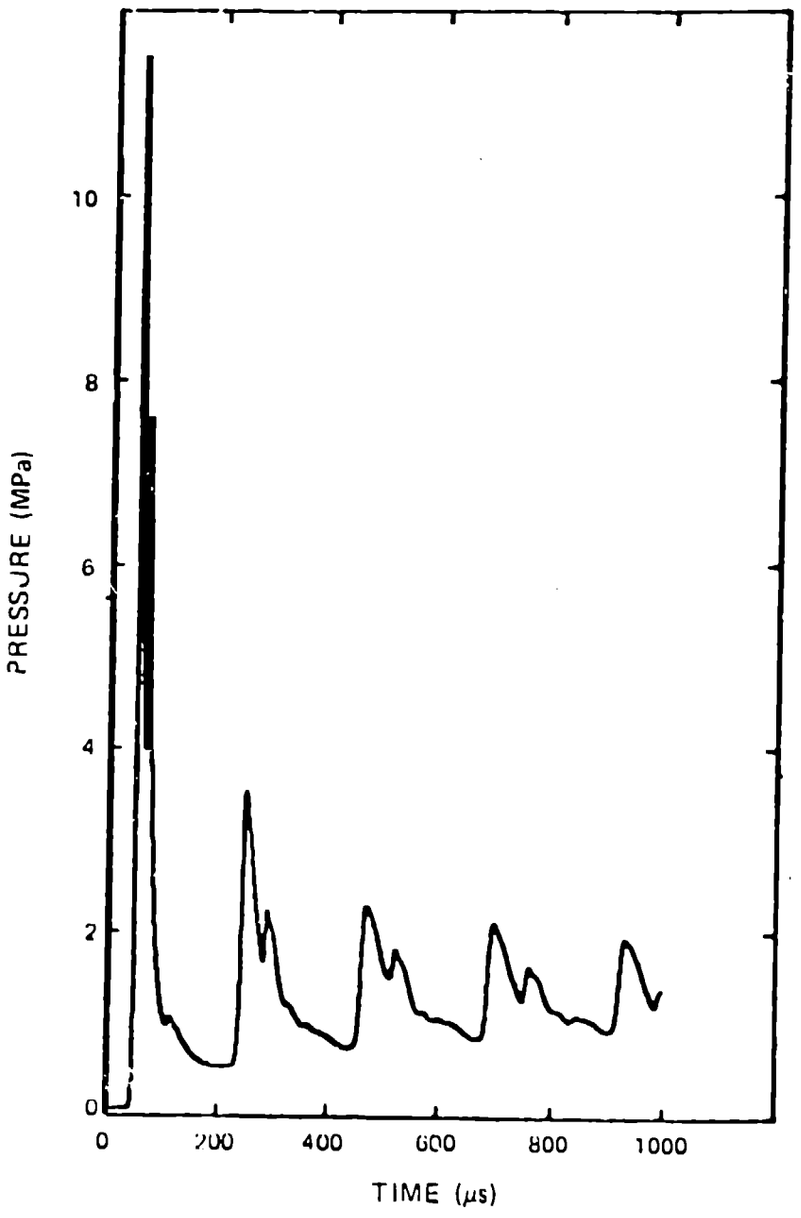


Fig. 7. Calculated pressure pulse acting on the vessel wall (0-1000 μs, configuration indicated in Figure 4a).

pulse as well as several subsequent major loading pulses. A double-peaked structure caused by a wave reflection from the air-explosive interface is apparent within each major loading pulse.

A change in the relative size of the explosive charge changes the shape of the pressure pulse applied to the vessel wall. The pressure pulse illustrated in Figure 6 was generated by an explosive charge whose radius was 7 percent of the vessel radius. Figure 8 shows how the shape of the first major loading pulse changes as the size of the explosive charge changes. With a charge that is 14 percent of the vessel radius, the second pressure pulse, caused by the reflected wave, is larger than the initial pressure pulse, caused by the arrival of the main shock front.

## Comparisons of Measured and Computed Pressure Histories

Comparisons between measured and numerically calculated pressure pulses are illustrated in Figures 9, 10, and 11. For the two tests conducted with the vessel containing air at normal density, Figures 9 and 10, a good qualitative agreement is indicated between measurements and calculations. However, the calculated pressures appear to be quantitatively higher than the measurements. For the calculation of an evacuated vessel, Figure 11, complete air evacuation was assumed. For this experiment, however, an initial air pressure of about 100 Pa existed in the vessel. The calculations indicate that a high-pressure spike arrives at the vessel wall before the main pressure pulse. This pressure spike

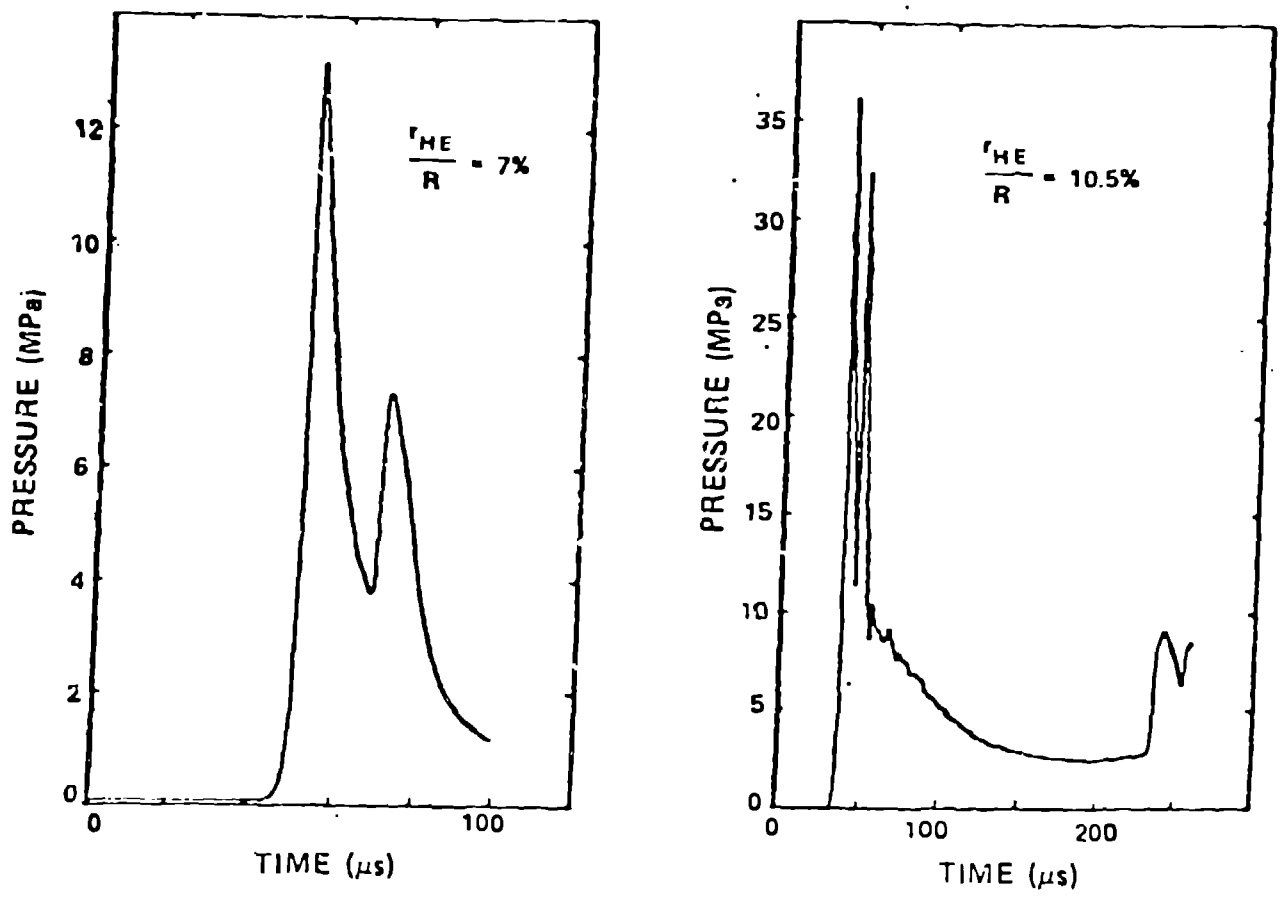


Fig. 8. Calculated pressure pulses for various size explosive charges.

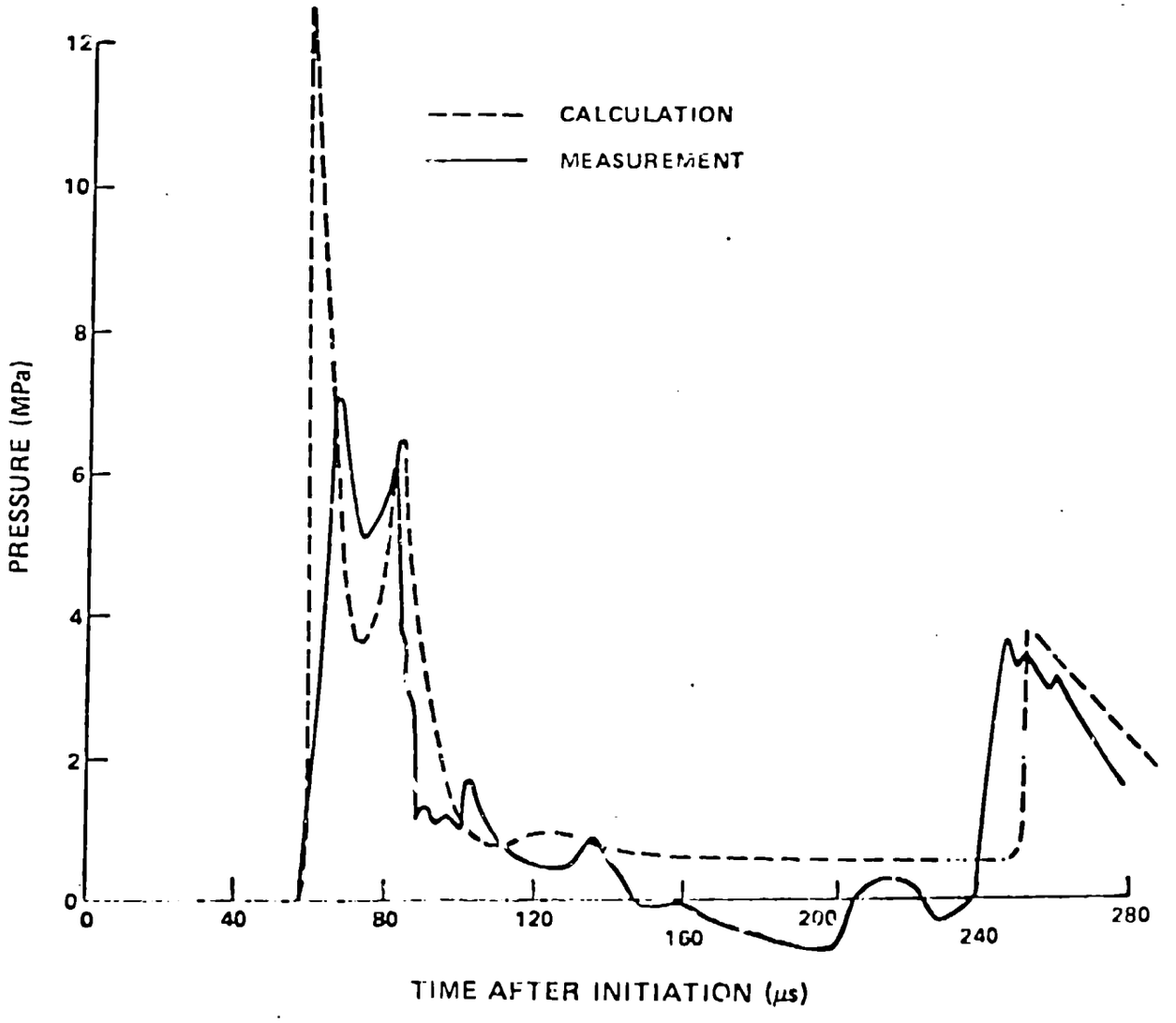


Fig. 9. Comparison of measured and calculated pressure acting on the vessel wall (parameters indicated in Figure 4a).

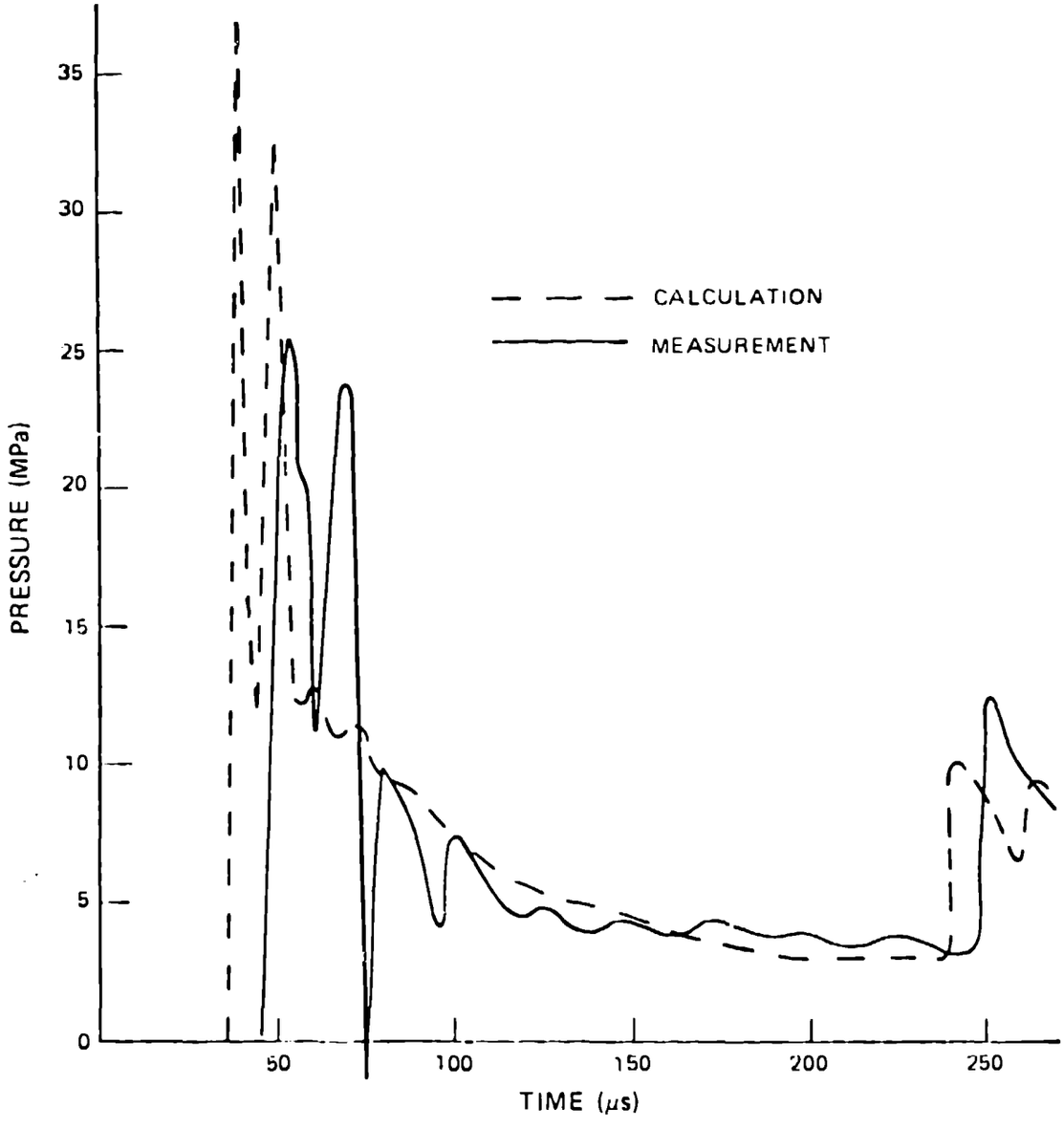


Fig. 10. Comparison of measured and calculated pressure acting on the vessel wall (38.1-mm-diam explosive charge, other parameters indicated in Figure 4a).

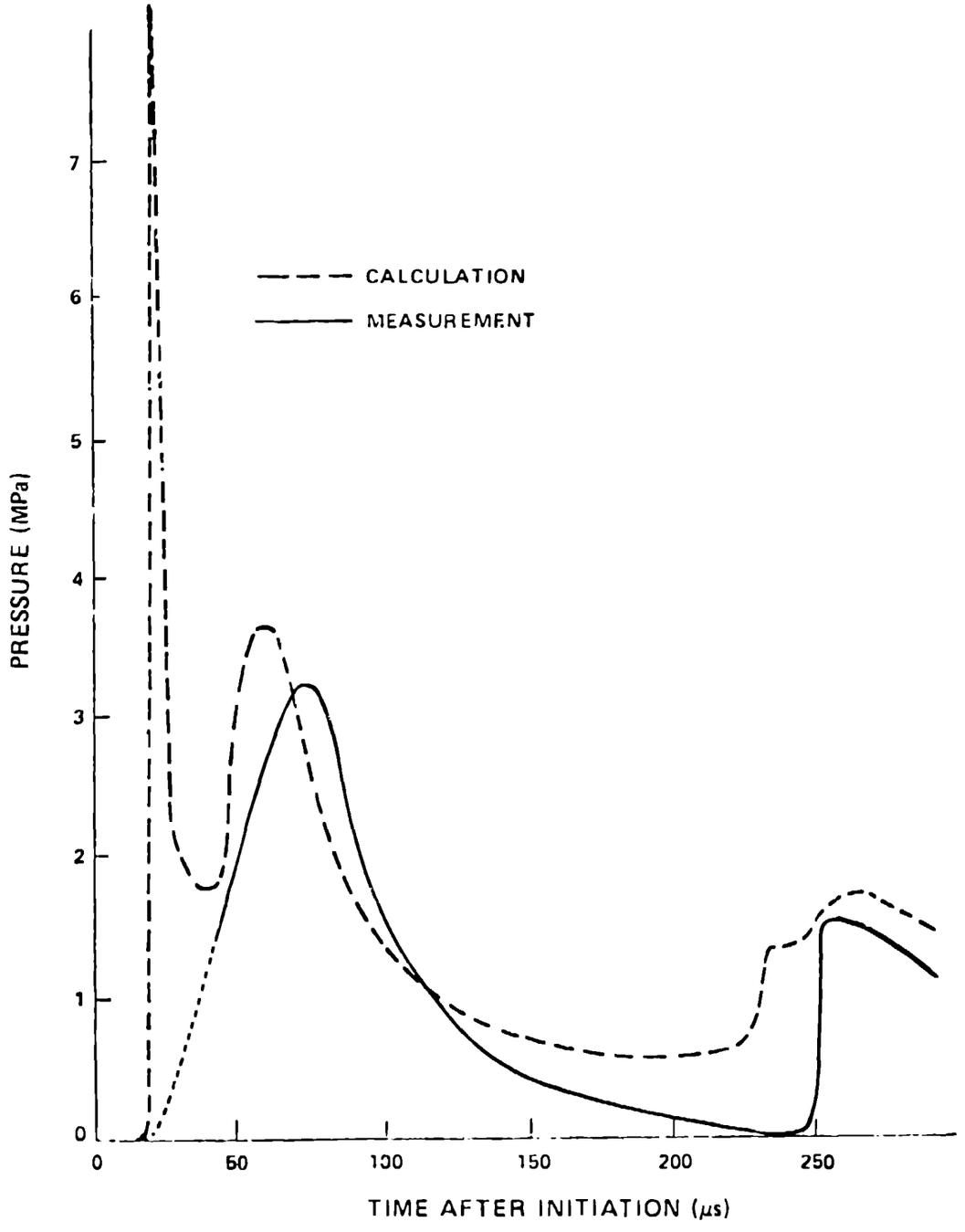


Fig. 11. Comparison of measured and calculated pressure acting on the vessel wall ($\rho_0$ = 1 g/m$^3$ vacuum case, other parameters indicated in Figure 4a).

is quite high in magnitude but short in duration and may be an artificial result of the numerical method. The experimental records show some high-frequency, high-pressure pulses; these are attributed to an air shock, since the vessel is not completely evacuated. Because the pressure-gauge response is not sufficient to resolve this high-frequency behavior at the beginning of the pressure pulse, the initial high-frequency data have been ignored in the measured pressure pulse of Figure 11. Aside from the very early data, which may not be significant with respect to the vessel response, a good qualitative and quantitative agreement exists between measurements and calculations.

## RESPONSE OF VESSELS TO BLAST LOADING

### One-Dimensional Vessel Response

The equation of motion of a thin spherical shell, Equation (3), can be solved for any pressure loading by numerical integration. Figure 12 shows the resulting strain history obtained by integrating Equation (3) for the pressure loading illustrated in Figures 6 and 7. The first major loading pulse lasts about 50 μs and initiates the sinusoidal motion of the vessel wall. If no other pressure pulses were applied to the wall, the vessel would continue to oscillate at constant amplitude in the one-dimensional case. However, the second major pressure pulse arrives at the vessel wall at about 220 μs, when the vessel wall has expanded but is moving inward. Therefore, the second major pressure pulse opposes the motion of the vessel wall and reduces the oscillation amplitude. For the calculation illustrated in Figure 12, the decrease in the oscillation amplitude caused by the arrival of the second pressure pulse is approximately 40 percent. Subsequent pressure pulses increase the oscillation amplitude again; the amplitude at 1 ms is about 75 percent of the initial value. Figure 12 indicates the relative importance of the various pressure pulses that dynamically load the vessel wall. From these calculations, we find that the second major loading pulse causes a reduction in the oscillation amplitude for PBX-9404 charges whose radii are between 7 percent and 14 percent of the vessel radius. Other cases have not been explored.

Figure 13 shows a small-scale test vessel used to measure pressure and strain. Tests recently have been conducted with two

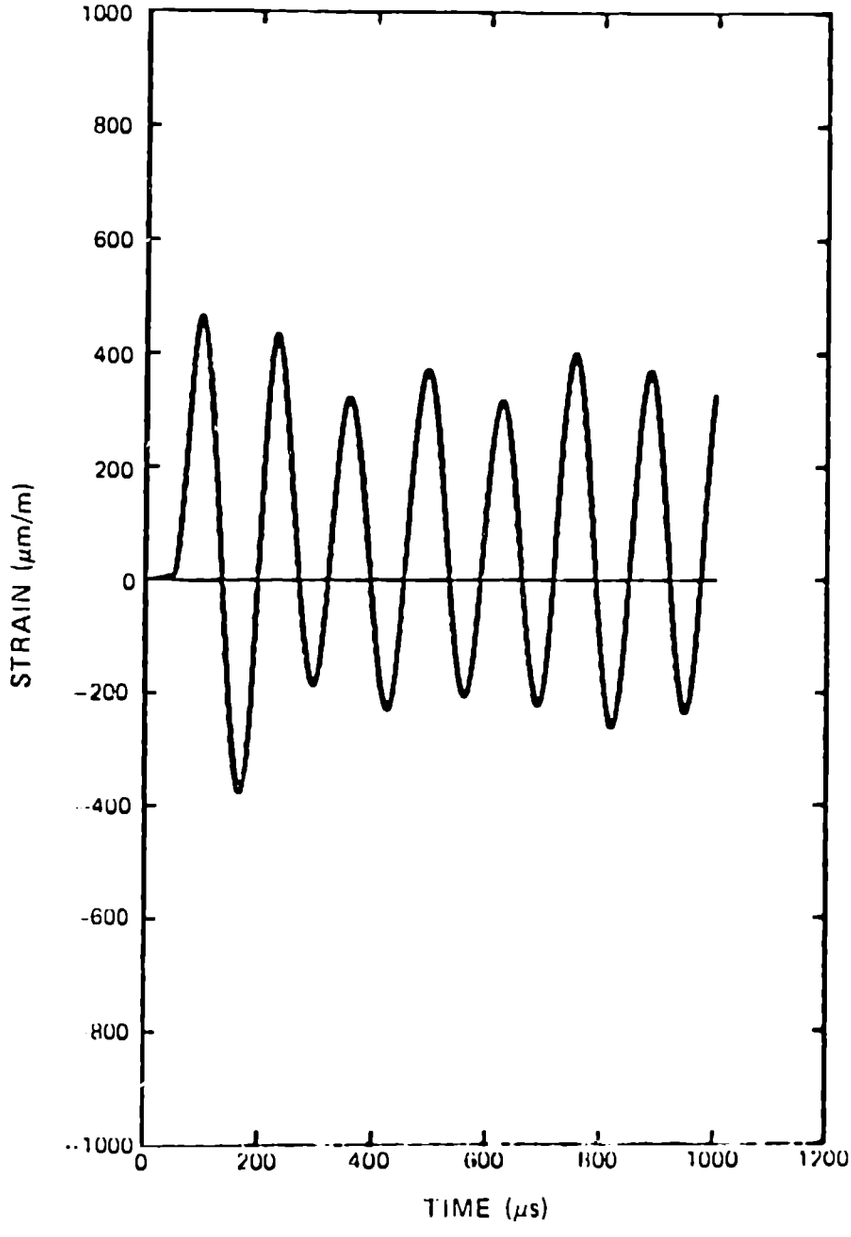


Fig. 12. Calculated strain based upon the one-dimensional shell theory (steel vessel with a 6.35-mm-thick wall, pressure loading shown in Figures 6 and 7).

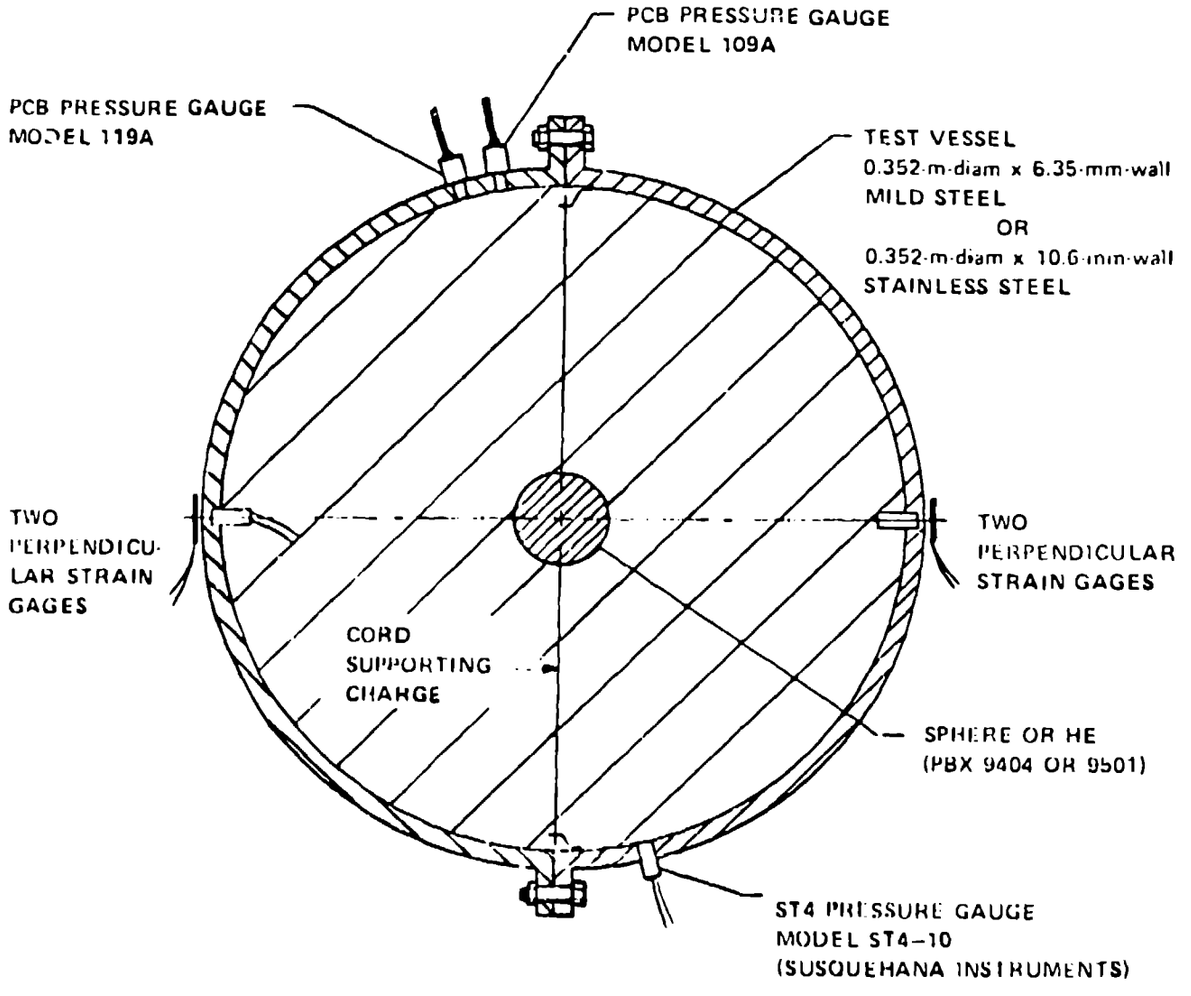


Fig. 13. Small-scale test vessel.

slightly different vessels, the thin-wall vessel (6.35-mm wall) illustrated in Figure 13 and a thick-wall vessel (10.6-mm wall). The thick-wall vessel is similar in design to the thin-wall vessel, but the flanges are considerably larger. Both vessels vibrate primarily in a two-dimensional mode. When the inside of the vessel wall is loaded by a spherically symmetric pressure pulse, the wall motion in the strain-gage area will be one-dimensional until a disturbance arrives from the flanges. From that time, the motion will be mainly two-dimensional. It takes about one-half period of the vessel's natural vibration for a wave to propagate from the flange area to the strain-gage area, so we would expect to observe a true one-dimensional motion at the strain gages for about the first half-cycle of vibration. For these test vessels, a valid comparison between calculated strains based on the assumption of spherically symmetric motion and measured strains can be made only for the first 60 μs of motion.

Figures 14, 15, and 16 compare the calculated and measured strain histories. Figure 14 shows the response of the thin-wall vessel to the detonation of a 25.4-mm-diam PBX-9404 charge when the vessel is filled with air at normal conditions. Comparing only the first strain pulse because the following motion will be perturbed by two-dimensional effects, we see that the calculated first peak strain is about 20 percent higher than the average of the four strain-gage measurements. However, the calculated value agrees quite well with strain-gage measurements 1 and 4. Figure 15 shows the response of the thick-wall vessel to the detonation of a

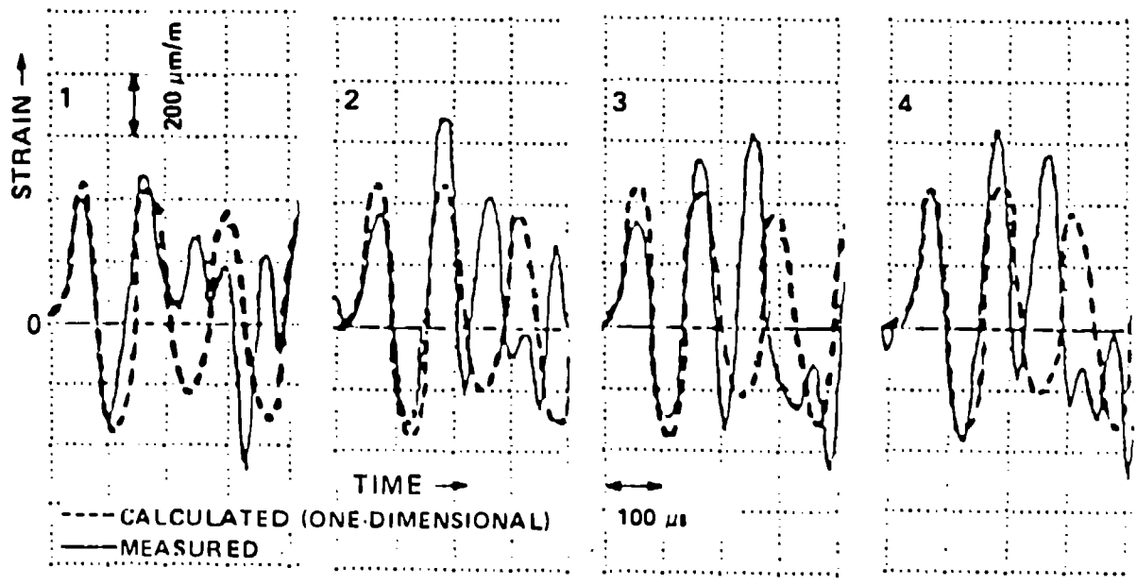


Fig. 14. Comparison of measured and calculated vessel strain, with the calculation based upon one-dimensional motion (0.352-m-diam vessel with a 6.35-mm-thick wall, 25.4-mm-diam PBX-9404 charge, air filled).

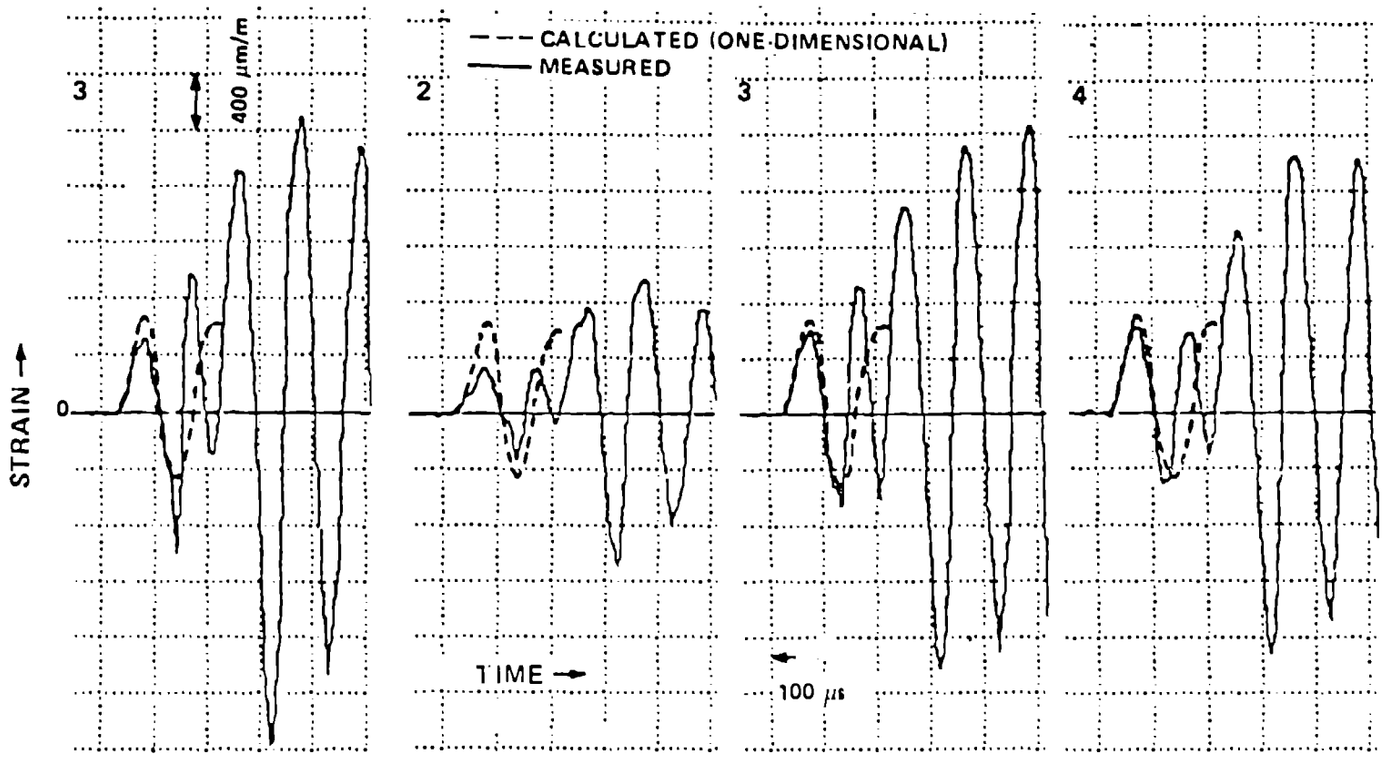


Fig. 15. Comparison of measured and calculated vessel strain, with the calculation based upon one-dimensional motion (0.352-m-diam vessel with a 10.6 mm-thick wall, 38.1 mm-diam charge, air filled).

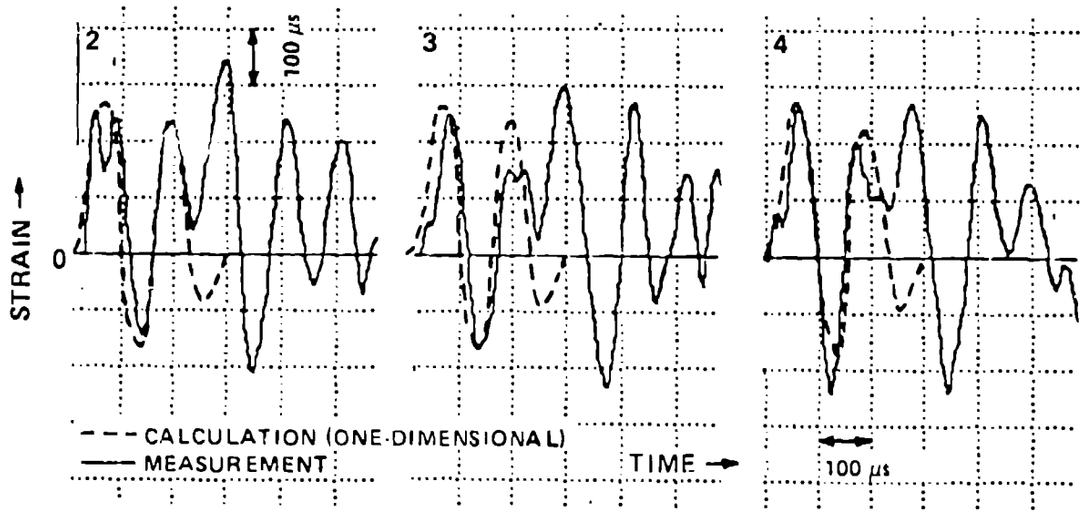


Fig. 16. Comparison of measured and calculated vessel strain, with the calculation based upon one-dimensional motion (0.352-m-diam vessel with a 6.35-mm-thick wall, 25.4-mm-diam charge, vacuum).

38.1-mm-diam PBX-9404/9501 charge when the vessel is filled with air at normal conditions. Again comparing only the first strain pulse, we see that the calculated peak is about 40 percent higher than the average of the strain-gage records, although the calculated value agrees quite well with gage records 3 and 4. Figure 16 shows the calculated and measured strains resulting from the detonation of a 25.4-mm-diam charge in a vessel that has been evacuated to about 100 Pa. The agreement between calculated and measured first peak strains is about 5 percent for all gages. In this test, the first peak strain was not indicated clearly by gage record number 1.

Generally, these calculations give reasonable estimates of the first peak strain amplitude. Even better estimates of the pressure loading and, therefore, better quantitative agreement between measured and calculated peak strains might be obtained by using calculations based upon extensively calibrated equations of state for both the explosive products and the air.

## Two-Dimensional Vessel Response

As indicated above, the motion of these test vessels is primarily two-dimensional (axially symmetric) because of the relatively large flanges, which induce significant axially symmetric perturbations to the spherical motion. Waves originating in the flange area converge at the spherical shell's poles, where the strain gages are mounted. The convergence increases the strain amplitude at the strain-gage location from two (thin-wall vessel) to five (thick-wall vessel) times the initial strain amplitude. This amplitude increase can be seen in the strain records of Figures 14 and 15.

To predict this fairly complicated motion, a two-dimensional analysis is required. Given the proper loading conditions, finite-element codes should be able to adequately simulate vessel response. By comparing these gage data with computational results we can assess the applicability of finite-element codes to dynamic pressure vessel design problems. The ADINA[12] finite-element code was chosen for this analysis because of its availability. Figure 17 shows the finite-element models, in the cylindrical coordinates R and Z, that were used to represent both thin-wall and thick-wall vessels. In the calculations, the shell structure of the vessel was represented by only one element across its thickness. The type of element used was the eight-node, axially symmetric element. A minimum number of elements was used to represent this vessel in the two-dimensional analysis because interest eventually will lie in analyzing three-dimensional vessels and extension to the three-dimensional problem then will not lead to decreased resolution.

Figure 18 shows the results of two ADINA code calculations for the motion of the thin-wall test vessel subjected to the internal pressure loading illustrated in Figures 6 and 7 (a 25.4-mm-diam explosive charge in an air-filled vessel). The results are the values of circumferential strain occurring at the center of the outside surface of the element near the hemisphere pole, where the strain gages are bonded to the vessel. In the fixed-flange calculation, we assumed that the flange bottom remained in contact with the symmetry plane ($z = 0$); see Figure 17. In the free-flange calculation, we assumed that the flange was free to move off the axis of symmetry. Because the flanges are held together by 24

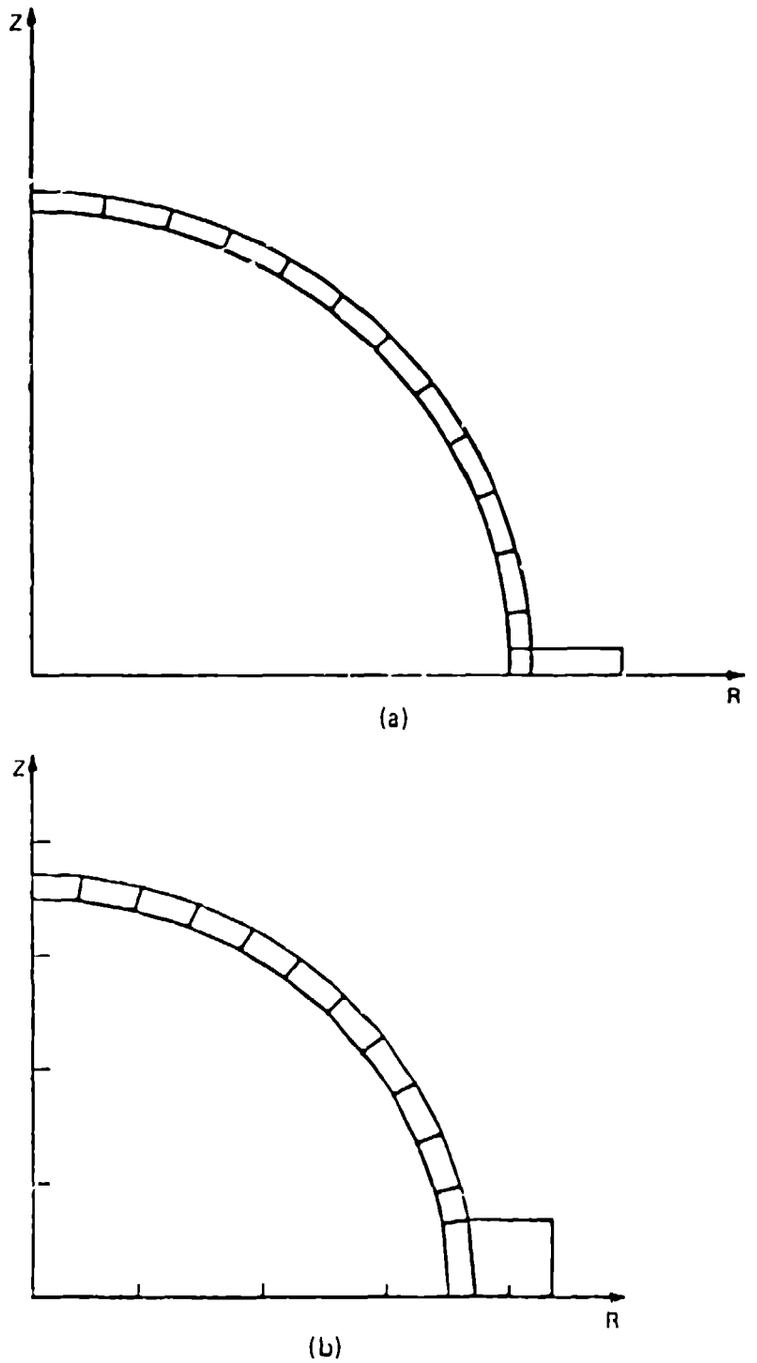


Fig. 17. Finite-element models used in the ADINA code to calculate the response of (a) the thin-wall test vessel and (b) the thick-wall test vessel.

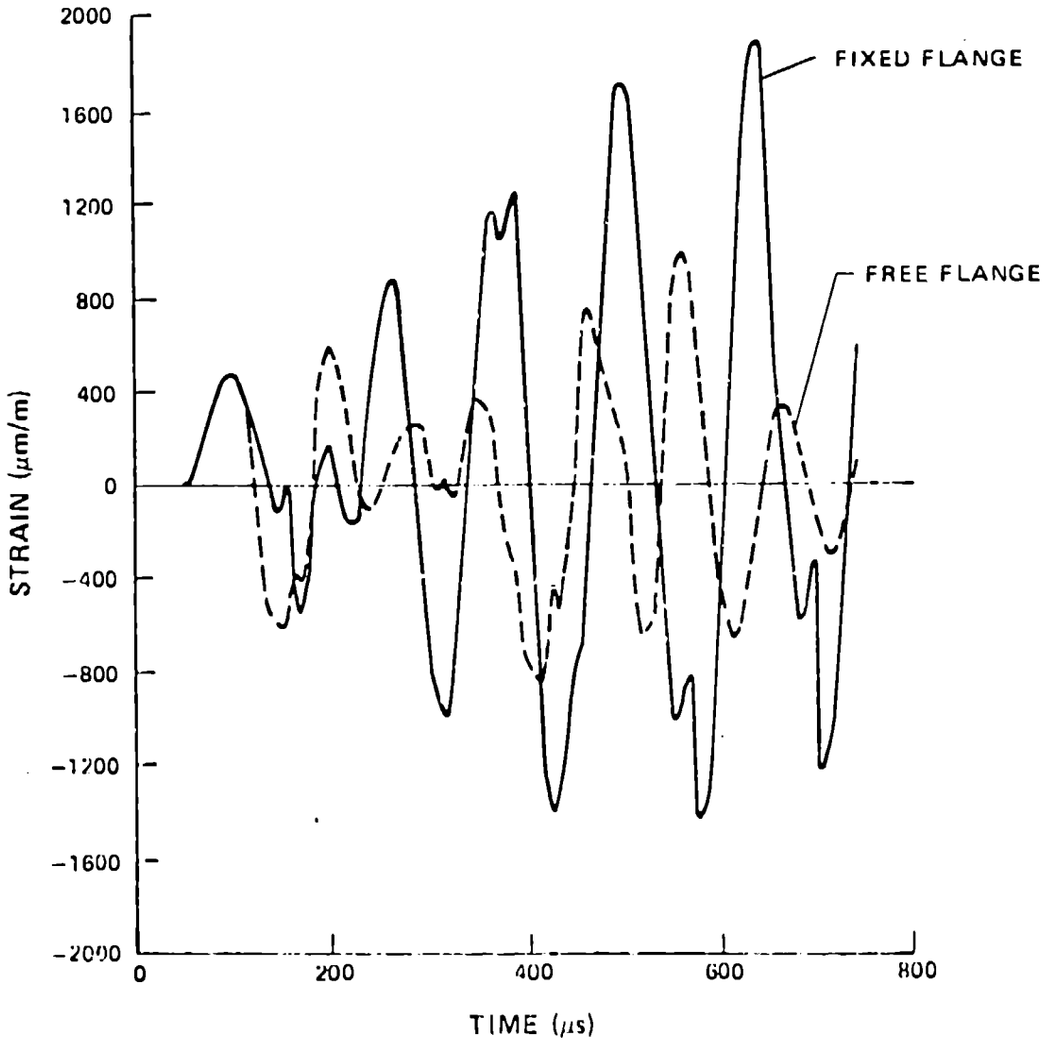


Fig. 18. The calculated response of a test vessel for free- and fixed-flange boundary conditions (0.352-m-diam vessel with a 6.35-mm-thick wall, 25.4-mm-diam PBX-9404 charge). Strain is measured in an element near the axis of symmetry in the circumferential direction.

equally spaced bolts, the true boundary condition to which the flange is subjected lies somewhere between these two extremes. From the results shown in Figure 18, we can conclude that the strain history at the vessel poles is a strong function of the boundary conditions applied to the flanges.

Figure 19 shows a comparison between the free-flange calculation of Figure 18 and a strain-gage measurement. The agreement is fairly good, especially in view of the fact that a calculated pressure loading was used as input and that a very coarse zoning was used. Notice that the strain-gage measurement is saturated at about 550 μs, about the time when the calculated strain reaches its absolute maximum. A linear elastic analysis was used in ADINA because the strain amplitude was relatively low. A comparison between the fixed-flange calculation, Figure 18, and the strain-gage measurement, Figure 19, shows relatively poor agreement. Because the flange on the thin-wall vessel is relatively thin, it would be expected that the free-flange calculations would agree with the experiment better than the fixed-flange calculations agree.

Figure 20 illustrates the results of an ADINA calculation for the thick-wall test vessel motion caused by the detonation of a 38.1-mm-diam explosive charge in an air-filled vessel. Shown are the initial configuration and the displaced configuration at 60, 130, and 200 μs after application of the loading pulse. The displacement has been multiplied by 200 to make the motion visible. The initial corner position of each element is indicated by a dot.

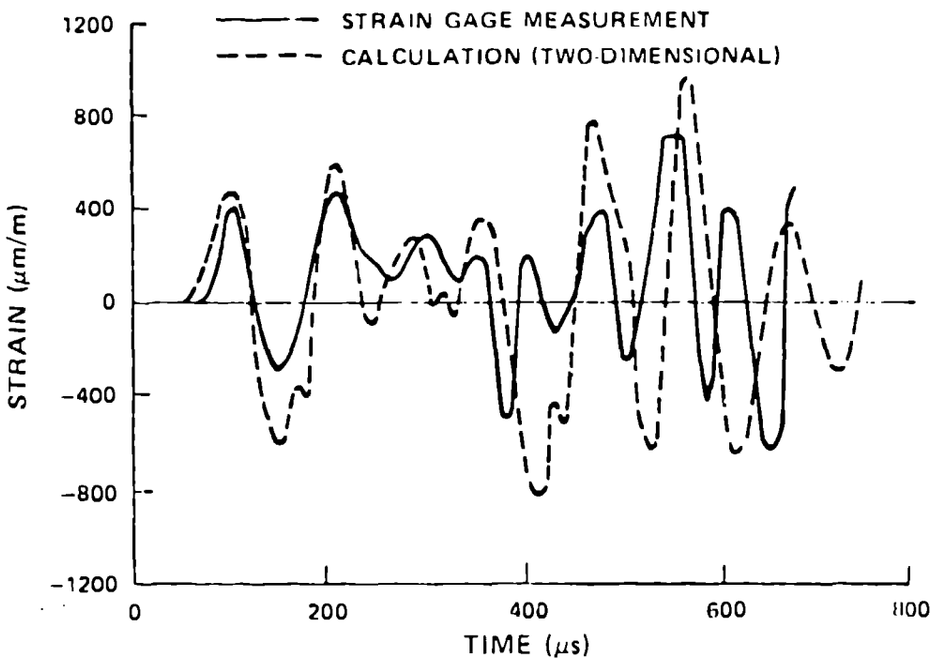


Fig. 19. Comparison between calculated and measured strain in the vessel wall near the axis of symmetry (01352-m-diam vessel with a 6.35-mm-thick wall, 25.4-mm-diam PBX-9404 charge).

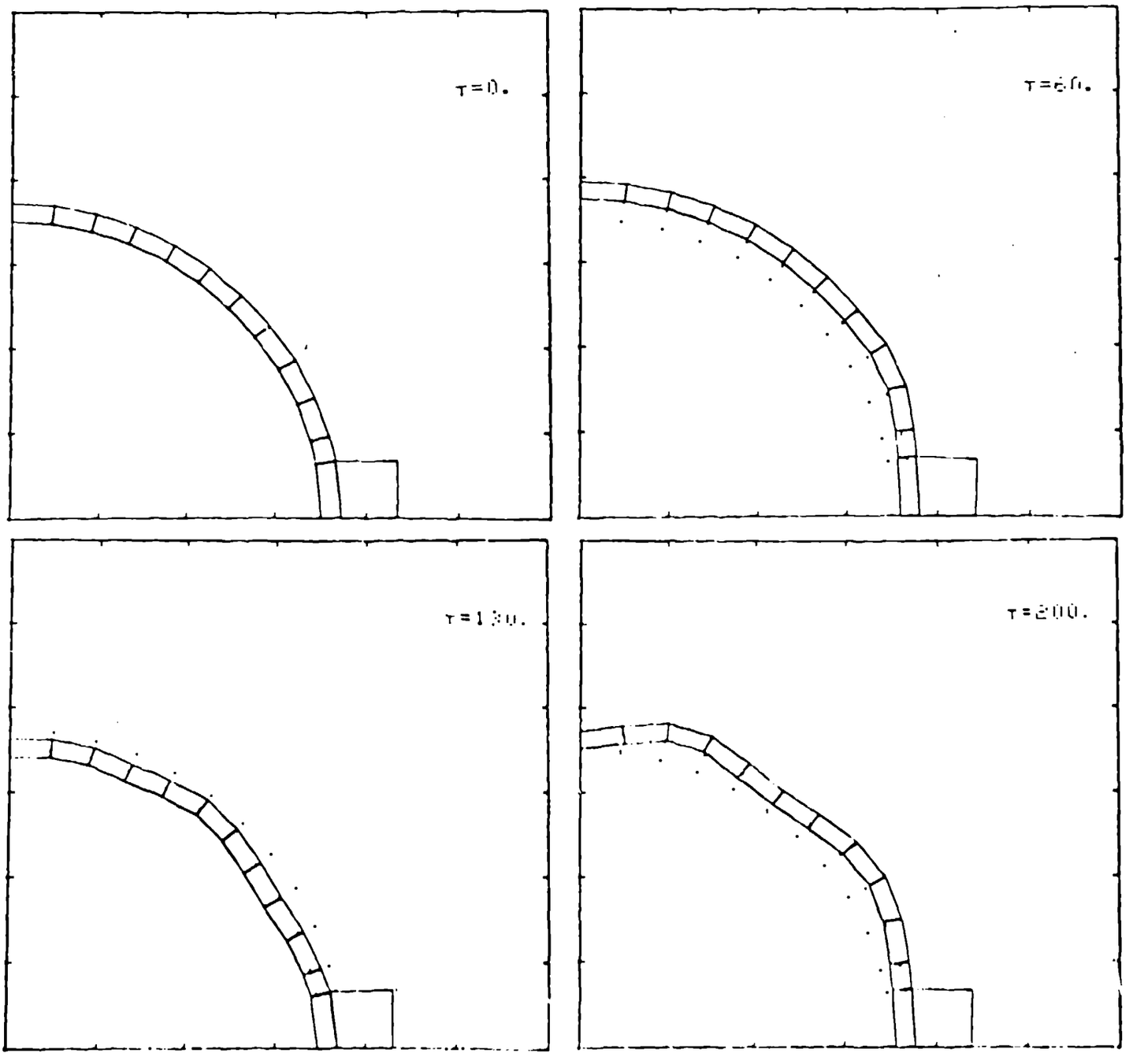


Fig. 20. The displaced configuration of a test vessel, at selected times, as calculated by ADINA (0.352-m-diam vessel with a 10.6-mm-thick wall, 38.1-mm-diam PBX-9404/9501 charge). The displacement has been multiplied by 200.

At 60 μs, we see both the perfectly spherical motion of the vessel's upper portion and a wave propagating from the flange toward the vessel pole. After 130 μs, the motion is far from spherical, and there is significant bending motion in the vessel.

Figure 21 shows the agreement between measured and calculated strain at the strain-gage locations. The calculation was performed with the fixed-flange boundary condition. Because the thick-wall test vessel has a massive flange, the fixed-flange condition should represent the physical configuration somewhat better than the free-flange condition does. An elastic-plastic material model was used because the strains attain a fairly high level. The yield strength, which was used in the von Mises yield criterion, was taken as 207 MPa. A work hardening modulus of 20.7 GPa was used in the isotropic hardening model of ADINA. This value is 10 percent of Young's modulus. Agreement between calculated and measured strain is good. However, a phase shift occurs at about 500 μs; significant yielding occurs in the strain-gage area shortly before the phase shift.

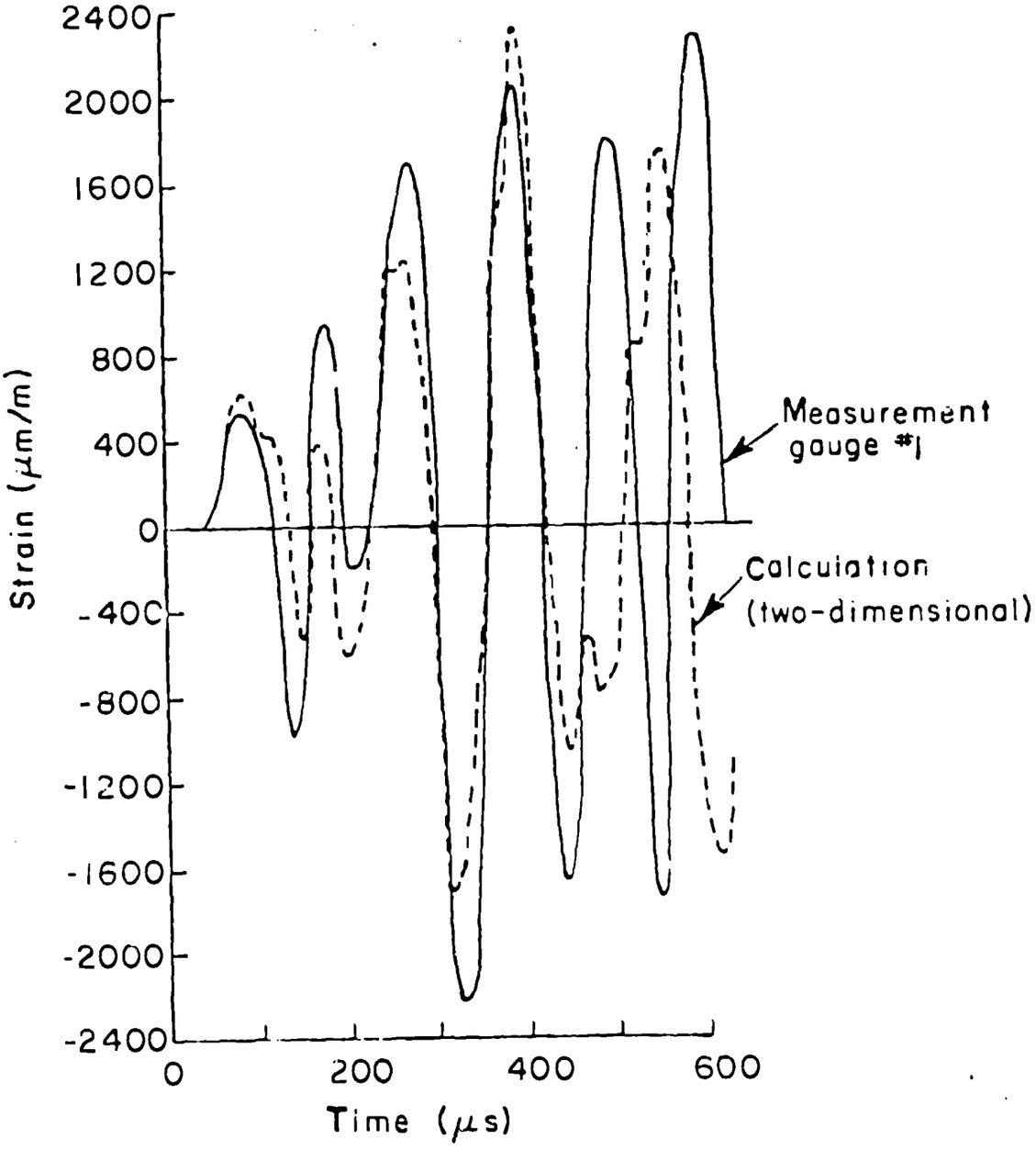


Fig. 21. Comparison between calculated and measured strain in the vessel wall near the axis of symmetry (0.352-m-diam vessel with a 10.6-mm-thick wall, 38.1-mm-diam PBX-9404/9501 charge).

## CONCLUSIONS

The sensitivity of the peak strain to the shape of the blast-wave pressure pulse has been investigated in a spherical vessel undergoing one-dimensional motion. As expected, the peak strain decreases rapidly when the pressure pulse is spread over a time longer than about a quarter period of the vessel's natural vibration.

Details of the blast-wave pressure pulse delivered to the vessel wall, analyzed with a one-dimensional, finite-difference code, show a fairly complex pulse structure. Calculated pressure loadings agree reasonably well with pressure gauge measurements. Vessel strain histories have been calculated with both one- and two-dimensional computer codes, and agreement between calculated results and strain-gage measurements is good. This result demonstrates the usefulness of these standard calculational techniques as design tools.

## REFERENCES


1. Karpp, R.R., Duffey, T.A., and Neal, T.R., "Response of Containment Vessels to Explosive Loading", Los Alamos Scientific Laboratory, Los Alamos, NM. LA-8082,June 1980.

2. Baker, W. E., Hu, W. C. L., and Jackson, T. R., "Elastic Response of Thin Spherical Shells to Axisymmetric Blast Loading," Journal of Applied Mechanics, Vol. 33, No. 4, pp. 800-806, December 1966.

3. Demchuk, A. F., "Method for Designing Explosion Chambers," Zhurnal Prikladnoi Mekhaniki i Technicheskoi Fiziki, Vol. 9, No. 5, pp. 47-50, 1968.

4. Ivanov, A. G., Novikov, S. A., and Sinitsyn, V. A., "The Behavior of Steel Shells When Charges of Explosive Detonate Inside Them," Zhurnal Prikladnoi Mekhaniki i Tekhnicheskoi Fiziki, Vol. 9, No. 6, pp. 94-98, 1968.

5. Buzukov, A. A., "Characteristics of the Behavior of the Walls of Explosion Chambers Under the Action of Pulsed Loading," Fizika Goreniya i Vzryva, Vol. 12, No. 4, pp. 605-610, July-August 1976.

6. Trott, B. D., Backofen, J. E., White, J. J., and Petty, J., "Design of Explosive Blast Containment Vessels for Explosive Ordnance Disposal Units," Proceedings of the Army Symposium on Solid Mechanics, 1978, Army Materials and Mechanics Research Center, Watertown, MA, AMMRC MS 78-3, pp. 215-228, September 1978.

7. White, J. J., and Trott, B. D., "Scaling Law for the Elastic Response of Spherical Explosion-Containment Vessels," Experimental Mechanics, Volume 20, No. 5, pp. 174-177, May 1980.

8. Fickett, W., PAD, A One-Dimensional Lagrangian Hydrocode, Los Alamos Scientific Laboratory, Los Alamos, New Mexico, LA-5910-MS, April 1975.

9. Taylor, G. I., "The Dynamics of the Combustion Products Behind Plane and Spherical Detonation Fronts in Explosives," Proc. Roy. Soc. (London) A, Vol. 200, p. 235, 1950.

10. Lee, E. L., Hornig, H. C., and Kury, J. W., Adiabatic Expansion of High Explosive Detonation Products, Lawrence Livermore Laboratory, Livermore, CA, UCRL-50422, May 1968.

11. Brode, H. L., "Blast Waves from a Spherical Charge," Physics of Fluids, Vol. 2, No. 2, p. 217, 1959.

12. Bathe, K. J., ADINA, A Finite Element Program for Automatic Dynamic Incremental Nonlinear Analysis, Massachusetts Institute of Technology, Cambridge, MA, No. 82448-1, September 1975.